Carbon 146 (2019) 486–490

Contents lists available at ScienceDirect

Carbon

journal homepage: www.elsevier.com/locate/carbon

Planar graphene-C_{60}-graphene heterostructure for sensitive UV-Visible photodetection

Shuchao Qin [a, 1], Hongzhu Jiang [a, 1], Qianqian Du [a], Zhonghui Nie [a], Xinran Wang [a], Wenjun Wang [b], Xizhang Wang [c], Yongbing Xu [a], Yi Shi [a], Rong Zhang [a], Fengqiu Wang [a, *]

[a] School of Electronic Science and Engineering and Key Laboratory of Intelligent Optical Sensing and Manipulation, Ministry of Education, Nanjing University, 210093, China
[b] Key Laboratory of Optical Communication Science and Technology of Shandong Province, School of Physical Science and Information Engineering, Liaocheng University, 34 Wenhua Road, Liaocheng, 252059, China
[c] School of Chemistry and Chemical Engineering, Nanjing University, 163 Xianlin Avenue, Nanjing, 210093, China

ARTICLE INFO

Article history:
Received 4 December 2018
Received in revised form
21 January 2019
Accepted 16 February 2019
Available online 18 February 2019

ABSTRACT

Low-dimensional organic materials have attracted intense attention due to their potential applications in low-cost, flexible electronics and optoelectronics. C_{60} has shown promise for high-performance photodetectors due to its strong light-matter interactions. However, limited by its poor crystallinity on oxide substrates and short exciton diffusion length, the potential of pristine C_{60} as photodetector channel material has not been fully exploited. Here, we fabricated a graphene-C_{60}-graphene photoconductor, where well-crystallized C_{60} film is obtained on a hexagonal boron nitride (h-BN) template and the two graphene sheets function as source and drain electrodes. The all-carbon device covers ultraviolet (UV) to near-infrared (200–800 nm), and the photoresponsivity reaches up to 5510 A W^{-1}@360 nm and 2280 A W^{-1}@405 nm, with an operating bandwidth of ~6 kHz. In addition, the gate-tunable graphene/C_{60} interface barrier enables an adjustable responsivity. Our results confirm the potential of pristine C_{60} as highly-sensitive photon sensor and video-frame-rate imaging application for the UV-Visible band.

1. Introduction

Organic molecules have received renewed interest in electronics and optoelectronics because of their excellent mechanical flexibility, large-scale yields, low manufacturing costs and diversified bandgap selection [1–4]. Recently, self-assembly of organic molecules on emerging two-dimensional (2D) materials, such as graphene, opens up new possibilities for exploring emerging low-dimensional phenomena as well as novel device applications [5–7]. Among various organic materials, zero-dimensional (0D) C_{60} exhibits strong absorption in the ultraviolet-visible range, allowing the fabrication of high-performance broadband photodetectors [7–9]. In our previous work, highly sensitive and robust UV photodetector has been demonstrated by the self-assembled of C_{60} on graphene sheet [7]. However, due to the use of graphene as the conducting channel and a photogating mechanism, the device exhibits rather high dark current. In addition, the long lifetime of carriers localized in C_{60} significantly limits the operation bandwidth.

Compared with graphene, the moderate bandgap of C_{60} films allows for suppressed dark current and low noise photodetection, making it an ideal candidate for photoconductor channel material. Furthermore, it is likely to realize a fast response time due to the ultrafast photocarrier relaxation dynamics of C_{60}. Unfortunately, the intrinsic performance of pristine C_{60}, in the context of optoelectronic device, has rarely been evaluated. This is limited by the forceful intermolecular cohesion which leads to a severe 'molecular non-wettability' issue when growing C_{60} films on oxide dielectrics [10]. The stochastic grain boundaries in polycrystalline organic films and interficial trap sites would dramatically suppress their charge transport. Consequently, C_{60} has been employed either as a trapping material in optoelectronic applications [11,12] or formed the conjugated hybrids with other materials [13–16].

The h-BN, a 2D insulator, has proved a feasible strategy for studying organic films [6,17,18]. Being atomically flat without dangling bonds, h-BN provides an ideal substrate that may

* Corresponding author.
E-mail address: fwang@nju.edu.cn (F. Wang).
[1] These authors contributed equally to this work.

https://doi.org/10.1016/j.carbon.2019.02.051
0008-6223/

minimize the interficial charge traps and achieve a well-ordered structure [19]. The van der Waals interaction and intermolecular π-π stacking between the substrate and organic molecules enable the epitaxial growth of organic films, with increasing grain sizes and better carrier transport [5].

In this work, using h-BN as a molecular-wetting substrate, highly crystalline C_{60} film is directly assembled as a photoconductive channel in a planar graphene-C_{60}-graphene heterostructure device. The photodetection wavelength is broad, covering the UV-visible range (200–800 nm). Upon illumination, the device achieves a high photoresponsivity (5510 A W^{-1}@360 nm, 2280 A W^{-1}@405 nm) and a large operating bandwidth (~6 kHz). The superior photodetection figures-of-merit are attributed on one hand to the strong light-matter interaction in C_{60}, and on the other hand, the high electrical conductivity of graphene and the gate-tunable graphene/C_{60} interface barrier. The combination of high responsivity and fast response time makes the all-carbon photodetector well suited for video-frame-rate imaging applications.

2. Methods

2.1. Materials and fabrication of the devices

Graphene samples were grown on copper foil by chemical vapor deposition (CVD) method, and Raman spectroscopy combined with optical microscope characterizations point to a defect-free single-layer sample. The C_{60} solid (purity of 97% without further purification) is from a commercial supplier. The device fabrication started with an exfoliation of h-BN onto a Si/SiO_2 (285 nm) wafer. Then graphene samples were transferred onto the h-BN using the poly(methyl methacrylate) supported procedure. Subsequently, metal compositions (Ti/Pd/Au with the thickness of ~1/5/60 nm) as the collecting electrodes were patterned by standard electron-beam lithography (EBL) techniques using PMMA as the resist and then evaporated by the electron beam evaporation (EBE). We then patterned a 100 nm-width gap in graphene by another EBL and oxygen plasma etching, to form the source and drain electrodes. Finally, C_{60} film was deposited on h-BN substrate by a thermal evaporation process (~440 °C) under 2×10^{-4} Pa vacuum and an evaporating rate of ~0.7 nm/min, and similar growth procedure had been reported before [6].

2.2. Morphology, structure characterizations and electrical measurements

Atomic force microscopy (AFM) measurements were performed using a NT-MDT Spectrum Instruments AFM operating at room temperature and ambient conditions. Optical absorption spectrum was measured using a Hitachi UV-vis-3310 spectrophotometer. Raman and Photoluminescence (PL) measurements were performed in a Horiba Jobin Yvon LabRAM HR 800 system using a 514 nm excitation, × 100 objective lens with about 1 μm diameter spot size, and 1800 lines/mm grating with about 0.45 cm^{-1} spectral resolution. Unless otherwise stated, all electrical measurements were carried out by the Keithley 4200 parameter analyzer in a closed probe station under vacuum (10^{-6} Torr) at room temperature. For photoresponse characterization, we used 360, 405, 532 and 658 nm laser diodes, respectively. The beam was guided through an optical fiber with a FC/PC ferrule and was subsequently incident onto the channel of the devices without focusing.

3. Results and discussion

The morphology of the C_{60} films evaporated on h-BN/SiO_2 was first investigated using atomic force microscopy, as shown in Fig. 1a. AFM image of C_{60} film shows larger grain sizes (~75 nm) on h-BN sheet than that on SiO_2 (~30 nm), which is facilitated by the van der Waals interactions between C_{60} and h-BN. The morphologies of C_{60} deposited on different substrates confirm that h-BN can serve as an ideal dielectric layer for depositing well-ordered C_{60} structures (see Fig. S1, in the supporting information). The stronger PL signal of C_{60} grown on h-BN indicates the well-ordered nature of C_{60} deposition, which is consisted with the AFM results. Fig. 1c shows the UV-Visible absorption spectrum of the C_{60} film deposited on the surface of quartz glass, and the inset shows their real photograph. C_{60} film exhibits a broadband absorption range, especially in the UV region, indicating its potential for broadband photodetection. As dictated by its bandgap, the absorption is dramatically decreased beyond 620 nm [7]. Raman spectroscopy of C_{60} on h-BN was also performed, as shown in Fig. 1d. At room temperature, most prominent is the pentagonal pinch mode $A_g(2)$, located at 1468 cm^{-1}, which is identifiable even when the laser power is very low. The intensities of H_g modes in the high energy regime are much weaker at room temperature [20], while the $H_g(6)$, $H_g(7)$ and $H_g(8)$ modes in the become observable with the increase of the laser power.

Fig. 2a shows the graphene-C_{60}-graphene device schematic on a h-BN substrate. The false-colour scanning electron microscopy (SEM) image of the device is displayed in Fig. 2b. The graphene sheet, before the gap is patterned, shows a bipolar transfer curve (see Fig. S2 in the supplementary information). A representative transfer curve of the graphene-C_{60}-graphene device is shown in Fig. 2c, showing the n-channel C_{60}-based FET characteristics. The left-hand logarithm scale indicates an on-off ratio of ~10^6 at $V_{DS} = 10$ V. From the linear fit of a $I_{DS}^{1/2}$ versus V_G plot in the saturation region, a threshold voltage $V_{th} = 25$ V is derived. Fig. 2d shows the output curve of a representative device, where the slight but observable asymmetry is caused by a barrier between C_{60} and the graphene electrodes [5]. The energy level at the Dirac point of graphene is about 4.5–4.7 eV, which is lower than that of the lowest unoccupied molecular orbital (LUMO) of C_{60} (~4.3 eV), leading to an electron barrier from graphene to C_{60} (insets of Fig. 2d). At $V_G < V_{th}$, the high interfacial barrier and low carrier density in C_{60} pinch off this C_{60}-based FET. With higher V_G ($V_G > V_{th}$) applied, the carrier density in C_{60} is increased and the electron barrier is lowered, both leading to higher currents.

Fig. 3a shows the source-drain current (I_{DS}) of the device as a function of V_G under different illumination power of 405 nm. Evidently, the transfer curves under light illumination reveal substantial photo-induced current generation and modulation (see Fig. S3 in the supplementary information). The responsivity is defined as the ratio of photocurrent to the incident optical power ($R = I_{ph}/P_{in}$). The responsivities of the device for different gate bias are summarized in Fig. 3b. At smaller incident power (~0.01 nW), the photoresponsivities can vary by a ratio of 10^3 for different gate voltages. This feature demonstrates the potential of this device being used as a gate-tunable photodetector. This tunability is significant for detectors because it allows the control of the states (on-off) of the detector and adjustment of the required responsivity, depending on the light power intensity [21]. The large grain size of C_{60} can dramatically improve the charge carrier transport [6,10]. Indeed, it can also enhance the photoresponsivity of devices (see details in Fig. S4 of Supplementary Information). The gate-tunable behaviour of the device can be explained by a simple energy band diagram in Fig. 3c. Without any external bias voltage, the photo-generated electron-hole pairs excited in C_{60} would instantly recombine. In the presence of an external field, the band bending can promote the dissociation of the electron-hole pairs, and thus contribute to a higher photocurrent by an increased external bias voltage. For the OFF state ($V_G < V_{th}$), the higher barrier Φ_b at the

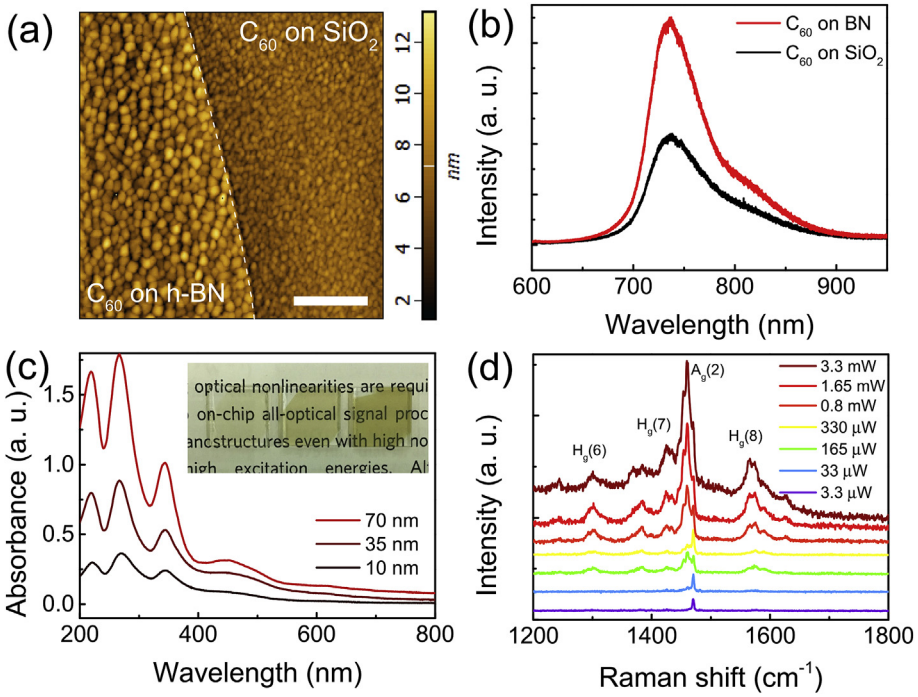

Fig. 1. (a) AFM image of C_{60} on h-BN or SiO_2/Si substrates, Scale bar, 500 nm. The white dot line marks the boundary of substrate with/without h-BN. (b) Photoluminescence spectra of C_{60} film (~70 nm) measured on h-BN or SiO_2/Si substrates. (c) The absorbance curves of C_{60} films with different thicknesses on quartz. Inset: the photographs of C_{60} films on quartz. (d) Raman spectra of C_{60} film (~70 nm) on h-BN under different laser power (514 nm). (A colour version of this figure can be viewed online.)

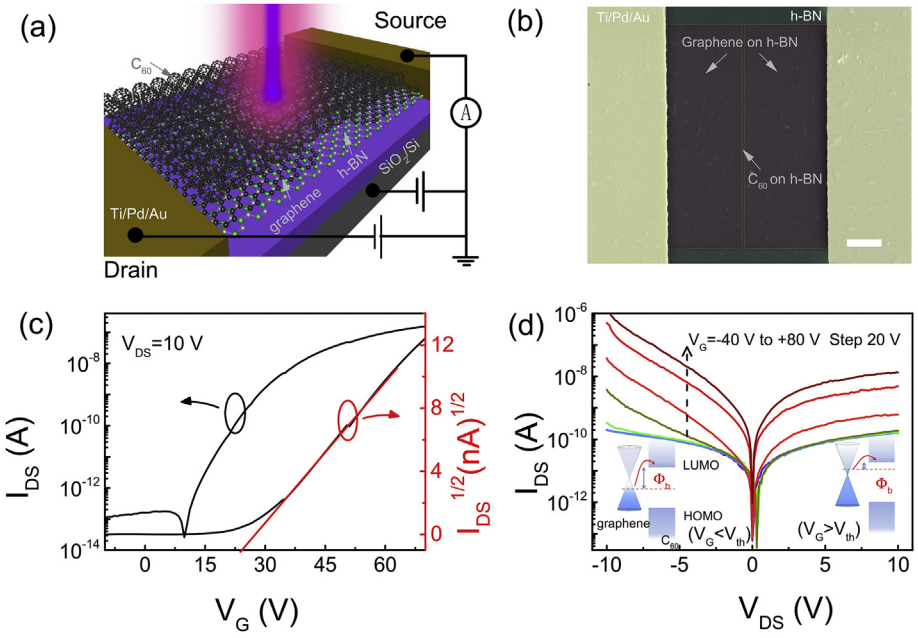

Fig. 2. (a) Schematic of the graphene-C_{60}-graphene device on h-BN/SiO_2/Si substrate. (b) The false-colour scanning electron microscopy (SEM) image of the graphene-C_{60}-graphene devices prepared on h-BN. Scale bar, 2 μm. (c) Transfer curves of graphene-C_{60}-graphene device at $V_{DS} = 10$ V. (d) Output curves at different gate voltages V_G. Insets show the gate-tunable energy diagram for the graphene-C_{60} contact. (A colour version of this figure can be viewed online.)

graphene/C_{60} contact depresses the photocurrent; Fermi level falls within the forbidden band of C_{60}, most electron-hole pairs would indirectly recombine with the assist of mid-gap defects or trap states, resulting in a negligible photocurrent. Due to the excellent electrical conductivity and a tunable Fermi energy level, graphene is widely employed as the contact electrode [22–24]. Here, the electron barrier height at the graphene/C_{60} contact can be lowered by increasing the gate bias V_G [25]. For the case of ON state ($V_G > V_{th}$), both thermionic and tunnelling currents contribute to the device currents [26]. The lowered barrier and filled defect/trap states at high gate bias would increase the efficiency of electron-hole pairs dissociation and extraction, contributing to a higher photoresponse.

To further confirm the capability of the all-carbon devices as

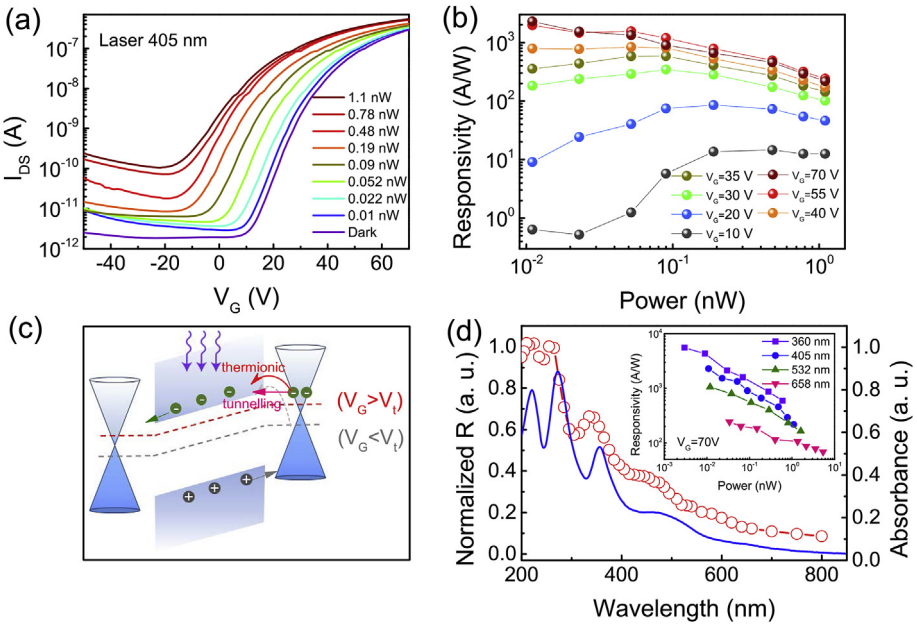

Fig. 3. (a) Transfer curves of the device in dark conditions and under various optical power densities provided by a 405 nm laser. (b) Responsivity of the device versus optical illumination power at different gate bias. (c) Schematic of gate-tunable energy band diagrams of the device under illumination. (d) Normalized spectral responsivity (red circles) of the device. The absorption (blue line) of the C_{60} film. Inset: responsivities as a function of the optical power density for UV and visible laser diodes. (A colour version of this figure can be viewed online.)

broadband photodetectors, we measured the spectral photoresponse from 200 to 800 nm. From the visible to the UV range, the photoresponsivity is seen to increase with incident photon energy (red circles in Fig. 3d), which is consistent with the absorption of the C_{60} film (blue lines). As limited by the bandgap of C_{60} film, the photoresponse is dramatically decreased for long wavelength range, and the photoresponse for the low photon radiation (>620 nm) mainly arises from the structural or compositional disorder [27]. The responsivity of the as-fabricated device is also measured by using several laser diodes covering UV and visible range (360, 405, 532, 658 nm, inset of Fig. 3d). Due to the strong light-matter interaction of C_{60}, the responsivity of the device can reach up to ~5510 A/W under low light intensity (~3 pW, 360 nm). We note that the responsivity does not saturate yet, so higher responsivity is expected under even lower laser power. In addition, due to the use of the all-carbon materials, advantages in terms of environmental robustness and compatibility with flexible substrates are directly inherent [7,28,29]. Combining with the advances in wafer-scale single-crystal h-BN film synthesis [30], such an all-carbon strategy is promising for future integrable UV optoelectronics.

Another key parameter of phototransistors is the response speed. The temporal photoresponse of the device was characterized using a pulsed laser at 405 nm. Fig. 4a shows the transient photocurrent of the graphene-C_{60}-graphene device measured at difference drain bias under an incident power of ~50 pW. The ON-OFF switching behaviour is robust and reproducible for the multiple cycles. In Fig. 4b, we verify these response times by ascertaining −3 dB bandwidth, a common figure-of-merit for photodetectors, by measuring the decline in photocurrent magnitude as the incident light signal is modulated with increasing frequency. A similar trend is shown for the different gate bias, where the photocurrents are normalized to the maximum value obtained at low modulation frequencies. The −3 dB bandwidth where the signal intensity has dropped to 70% of its initial value is about 5 kHz, implying the suitability for video-frame-rate imaging applications [31]. This operation speed can be attributed to the ultrafast photocarrier relaxation dynamics of C_{60} (~34 ps, see Fig. S5 in the supplementary information). At ambient air, the photoresponse of the device shows slight decrease as compared with the vaccum case, which is probably as a result of moisture or hydroxy group (see Fig. S6 in the supplementary information). The passivation by

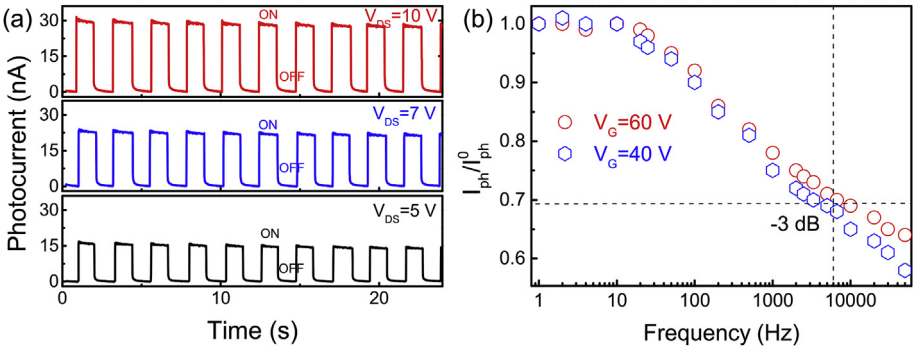

Fig. 4. (a) Temporal photocurrent response curves under a 405 nm laser for different drain bias at $V_G = 55$ V. (b) Normalized photoresponse as a function of light modulation frequency. (A colour version of this figure can be viewed online.)

covering the C_{60} surface with a protective layer such as Al_2O_3 is useful to maintain the high-performance for practical applications.

4. Conclusion

In summary, we fabricated a sensitive and fast all-carbon broadband photodetector (covering 200–800 nm) by employing highly-oriented crystalline C_{60} film on the molecular-wetting (h-BN) platform with graphene contact electrodes. The graphene-C_{60}-graphene device enables a high photoresponsivity (5510 A W^{-1}@360 nm, 2280 A W^{-1}@405 nm) with a desirable operating bandwidth of 5 kHz. In addition, utilizing work-function-tunable graphene as the contact electrodes can significantly modulate the responsivity of the device. Our strategy can also be extended to other organic semiconductor systems, in particular organic small molecules.

Acknowledgements

This work was supported in part by the State Key Project of Research and Development of China (2017YFA0206304), National Basic Research Program of China (2014CB921101); National Natural Science Foundation of China (61775093, 61427812, 61775089); National Youth 1000-Talent Plan; A 'Jiangsu Shuangchuang Team' Program; Natural Science Foundation of Jiangsu Province (BK20170012). Industrial Alliance Fund of Shandong Provincial Key Laboratory (SDKL2016038).

Appendix A. Supplementary data

Supplementary data to this article can be found online at https://doi.org/10.1016/j.carbon.2019.02.051.

References

[1] X. Liu, E.K. Lee, D.Y. Kim, H. Yu, J.H. Oh, Flexible organic phototransistor array with enhanced responsivity via metal-ligand charge transfer, ACS Appl. Mater. Interfaces 8 (11) (2016) 7291–7299.
[2] S. Zheng, X. Xiong, Z. Zheng, T. Xu, L. Zhang, T. Zhai, X. Lu, Solution-grown large-area C_{60} single-crystal arrays as organic photodetectors, Carbon 126 (2018) 299–304.
[3] X. Chen, X. Liu, B. Wu, H. Nan, H. Guo, Z. Ni, F. Wang, X. Wang, Y. Shi, X. Wang, Improving the Performance of graphene phototransistors using a heterostructure as the light-absorbing layer, Nano Lett. 17 (10) (2017) 6391–6396.
[4] C. Wang, H. Dong, W. Hu, Y. Liu, D. Zhu, Semiconducting π-conjugated systems in field-effect transistors: a material odyssey of organic electronics, Chem. Rev. 112 (4) (2012) 2208–2267.
[5] K. Kim, T.H. Lee, E.J.G. Santos, P.S. Jo, A. Salleo, Y. Nishi, Z. Bao, Structural and electrical investigation of C_{60} graphene vertical heterostructures, ACS Nano 9 (6) (2015) 5922–5928.
[6] T.H. Lee, K. Kim, G. Kim, H.J. Park, D. Scullion, L. Shaw, M.-G. Kim, X. Gu, W.-G. Bae, E.J.G. Santos, Z. Lee, H.S. Shin, Y. Nishi, Z. Bao, Chemical Vapor-deposited hexagonal boron nitride as a scalable template for high-performance organic field-effect transistors, Chem. Mater. 29 (5) (2017) 2341–2347.
[7] S. Qin, X. Chen, Q. Du, Z. Nie, X. Wang, H. Lu, X. Wang, K. Liu, Y. Xu, Y. Shi, R. Zhang, F. Wang, Sensitive and robust ultraviolet photodetector array based on self-assembled graphene/C_{60} hybrid films, ACS Appl. Mater. Interfaces 10 (44) (2018) 38326–38333.
[8] L. Du, X. Luo, F. Zhao, W. Lv, J. Zhang, Y. Peng, Y. Tang, Y. Wang, Toward facile broadband high photoresponse of fullerene based phototransistor from the ultraviolet to the near-infrared region, Carbon 96 (2016) 685–694.
[9] J. Han, J. Wang, M. Yang, X. Kong, X. Chen, Z. Huang, H. Guo, J. Gou, S. Tao, Z. Liu, Z. Wu, Y. Jiang, X. Wang, Graphene/organic semiconductor heterojunction phototransistors with broadband and bi-directional photoresponse, Adv. Mater. (2018), e1804020, https://doi.org/10.1002/adma.201804020.
[10] K. Itaka, M. Yamashiro, J. Yamaguchi, M. Haemori, S. Yaginuma, Y. Matsumoto, M. Kondo, H. Koinuma, High-mobility C_{60} field-effect transistors fabricated on molecular-wetting controlled substrates, Adv. Mater. 18 (13) (2006) 1713–1716.
[11] H. Zhou, J. Mei, M. Xue, Z. Song, H. Wang, High-stability, self-powered Perovskite photodetector based on a $CH_3NH_3PbI_3$/GaN heterojunction with C_{60} as an electron transport layer, J. Phys. Chem. C 121 (39) (2017) 21541–21545.
[12] B.C. Thompson, J.M. Frechet, Polymer-fullerene composite solar cells, Angew Chem. Int. Ed. Engl. 47 (1) (2008) 58–77.
[13] S. Park, S.J. Kim, J.H. Nam, G. Pitner, T.H. Lee, A.L. Ayzner, H. Wang, S.W. Fong, M. Vosgueritchian, Y.J. Park, M.L. Brongersma, Z. Bao, Significant enhancement of infrared photodetector sensitivity using a semiconducting single-walled carbon nanotube/C_{60} phototransistor, Adv. Mater. 27 (4) (2015) 759–765.
[14] X. Luo, L. Du, W. Lv, L. Sun, Y. li, Y. Peng, F. Zhao, J. Zhang, Y. Tang, Y. Wang, Charge-transport interfacial modification enhanced ultraviolet (UV)/near-UV phototransistor with high sensitivity and fast response speed, Synth. Met. 210 (2015) 230–235.
[15] D. Yang, X. Zhou, D. Ma, Fast response organic photodetectors with high detectivity based on rubrene and C_{60}, Org. Electron. 14 (11) (2013) 3019–3023.
[16] X. Wang, H. Li, Z. Su, F. Fang, G. Zhang, J. Wang, B. Chu, X. Fang, Z. Wei, B. Li, W. Li, Efficient organic near-infrared photodetectors based on lead phthalocyanine/C_{60} heterojunction, Org. Electron. 15 (10) (2014) 2367–2371.
[17] S.J. Kang, G.-H. Lee, Y.-J. Yu, Y. Zhao, B. Kim, K. Watanabe, T. Taniguchi, J. Hone, P. Kim, C. Nuckolls, Organic field effect transistors based on graphene and hexagonal boron nitride heterostructures, Adv. Funct. Mater. 24 (32) (2014) 5157–5163.
[18] K. Kim, E.J. Santos, T.H. Lee, Y. Nishi, Z. Bao, Epitaxially grown strained pentacene thin film on graphene membrane, Small 11 (17) (2015) 2037–2043.
[19] C.H. Lee, T. Schiros, E.J. Santos, B. Kim, K.G. Yager, S.J. Kang, S. Lee, J. Yu, K. Watanabe, T. Taniguchi, J. Hone, E. Kaxiras, C. Nuckolls, P. Kim, Epitaxial growth of molecular crystals on van der waals substrates for high-performance organic electronics, Adv. Mater. 26 (18) (2014) 2812–2817.
[20] M. Matus, H. Kuzmany, Raman spectra of single-crystal C_{60}, Appl. Phys. A 56 (1993) 241–248.
[21] G. Konstantatos, M. Badioli, L. Gaudreau, J. Osmond, M. Bernechea, F.P. Garcia de Arquer, F. Gatti, F.H. Koppens, Hybrid graphene-quantum dot phototransistors with ultrahigh gain, Nat. Nanotechnol. 7 (6) (2012) 363–368.
[22] S. Pyo, J. Choi, J. Kim, A Fully Transparent, flexible, sensitive, and visible-blind ultraviolet sensor Based on carbon nanotube-graphene hybrid, Adv. Electron. Mater. (2018) 1800737, https://doi.org/10.1002/aelm.201800737.
[23] S. Pyo, W. Kim, H. Jung, J. Choi, J. Kim, Heterogeneous integration of carbon-nanotube-graphene for high-performance, flexible, and transparent photodetectors, Small 13 (2017) 1700918.
[24] M. Kang, S.J. Kim, W. Song, S. Chang, C. Park, S. Myung, J. Lim, S.S. Lee, K. An, Fabrication of flexible optoelectronic devices based on MoS_2/graphene hybrid patterns by a soft lithographic patterning method, Carbon 116 (2017) 167–173.
[25] S. Qin, F. Wang, Y. Liu, Q. Wan, X. Wang, Y. Xu, Y. Shi, X. Wang, R. Zhang, A light-stimulated synaptic device based on graphene hybrid phototransistor, 2D Mater. 4 (3) (2017), 035022.
[26] H. Gao, J. Feng, B. Zhang, C. Xiao, Y. Wu, X. Kan, B. Su, Z. Wang, W. Hu, Y. Sun, L. Jiang, A.J. Heeger, Capillary-bridge mediated assembly of conjugated polymer arrays toward organic photodetectors, Adv. Funct. Mater. 27 (34) (2017) 1701347.
[27] Y. Wang, J.M. Holden, A.M. Rao, P.C. Eklund, U.D. Venkateswaran, D. Eastwood, R.L. Lidberg, G. Dresselhaus, M.S. Dresselhaus, Optical absorption and photoluminescence in pristine and photopolymerized C_{60} solid films, Phys. Rev. B 51 (7) (1995) 4547–4556.
[28] Y. Liu, Y. Liu, S. Qin, Y. Xu, R. Zhang, F. Wang, Graphene-carbon nanotube hybrid films for high-performance flexible photodetectors, Nano Res. 10 (6) (2016) 1880–1887.
[29] Y. Liu, F. Wang, X. Wang, X. Wang, E. Flahaut, X. Liu, Y. Li, X. Wang, Y. Xu, Y. Shi, R. Zhang, Planar carbon nanotube-graphene hybrid films for high-performance broadband photodetectors, Nat. Commun. 6 (2015) 8589.
[30] J.S. Lee, S.H. Choi, S.J. Yun, Y.I. Kim, S. Boandoh, J.-H. Park, B.G. Shin, H. Ko, S.H. Lee, Y.-M. Kim, Y.H. Lee, K.K. Kim, S.M. Kim, Wafer-scale single-crystal hexagonal boron nitride film via self-collimated grain formation, Science 362 (6416) (2018), 817-382.
[31] J.D. Mehew, S. Unal, E. Torres Alonso, G.F. Jones, S. Fadhil Ramadhan, M.F. Craciun, S. Russo, Fast and highly sensitive ionic-polymer-Gated WS_2-Graphene photodetectors, Adv. Mater. 29 (23) (2017) 1700222.